Sensors **2012**, *12*, 3669-3692; doi:10.3390/s120303669

OPEN ACCESS

sensors

ISSN 1424-8220

www.mdpi.com/journal/sensors

Article

Vapochromic Behaviour of $M[Au(CN)_2]_2$-Based Coordination Polymers (M = Co, Ni)

Julie Lefebvre, Jasmine L. Korčok, Michael J. Katz and Daniel B. Leznoff *

Department of Chemistry, Simon Fraser University, 8888 University Drive, Burnaby, BC V5A 1S6, Canada; E-Mails: jlefebvr@ucalgary.ca (J.L.); jkorcok@tru.ca (J.L.K.); mjkatz@sfu.ca (M.J.K.)

* Author to whom correspondence should be addressed; E-Mail: dleznoff@sfu.ca; Tel.: +1-778-782-4887; Fax: +1-778-782-3765.

Received: 10 February 2012; in revised form: 9 March 2012 / Accepted: 13 March 2012 / Published: 16 March 2012

Abstract: A series of $M[Au(CN)_2]_2(analyte)_x$ coordination polymers (M = Co, Ni; analyte = dimethylsulfoxide (DMSO), N,N-dimethylformamide (DMF), pyridine; x = 2 or 4) was prepared and characterized. Addition of analyte vapours to solid $M(\mu\text{-}OH_2)[Au(CN)_2]_2$ yielded visible vapochromic responses for M = Co but not M = Ni; the IR ν_{CN} spectral region changed in every case. A single crystal structure of $Zn[Au(CN)_2]_2(DMSO)_2$ revealed a corrugated 2-D layer structure with *cis*-DMSO units. Reacting a Ni(II) salt and $K[Au(CN)_2]$ in DMSO yielded the isostructural $Ni[Au(CN)_2]_2(DMSO)_2$ product. $Co[Au(CN)_2]_2(DMSO)_2$ and $M[Au(CN)_2]_2(DMF)_2$ (M = Co, Ni) complexes have flat 2-D square-grid layer structures with *trans*-bound DMSO or DMF units; they are formed via vapour absorption by solid $M(\mu\text{-}OH_2)[Au(CN)_2]_2$ and from DMSO or DMF solution synthesis. $Co[Au(CN)_2]_2(pyridine)_4$ is generated via vapour absorption by $Co(\mu\text{-}OH_2)[Au(CN)_2]_2$; the analogous Ni complex is synthesized by immersion of $Ni(\mu\text{-}OH_2)[Au(CN)_2]_2$ in 4% aqueous pyridine. Similar immersion of $Co(\mu\text{-}OH_2)[Au(CN)_2]_2$ yielded $Co[Au(CN)_2]_2(pyridine)_2$, which has a flat 2-D square-grid structure with *trans*-pyridine units. Absorption of pyridine vapour by solid $Ni(\mu\text{-}OH_2)[Au(CN)_2]_2$ was incomplete, generating a mixture of pyridine-bound complexes. Analyte-free $Co[Au(CN)_2]_2$ was prepared by dehydration of $Co(\mu\text{-}OH_2)[Au(CN)_2]_2$ at 145 °C; it has a 3-D diamondoid-type structure and absorbs DMSO, DMF and pyridine to give the same materials as by vapour absorption from the hydrate.

Keywords: vapochromism; cyanide; X-ray structures; cobalt(II); nickel(II)

---

1. Introduction

Vapochromic materials, which display colour (optical absorption) or luminescence changes upon exposure to vapours of volatile organic compounds (VOCs), are of great interest due to their potential applications for chemical vapour detection [1–16]. Such sensors are commercially important as environmental monitoring devices, as safety systems in industrial settings and for defence and security applications [17]. As an example of a vapochromic material, the polymeric Prussian Blue-type $Co^{2+}/[Re_6Q_8(CN)_6]^{4-}$ (Q = S, Se) material yields dramatic changes in the visible spectrum when exposed to specific VOCs; the colour changes are linked to the sensed solvent impacting the geometry and hydration around the Co(II) centres [12]. A range of compounds based on Au(I), Pd(II) and Pt(II) coordination polymers have also been extensively investigated for their vapochromic responses [1–12,14]. The vapochromism in these systems is based on changes in both the visible absorption and emission spectra. In the linear $\{Tl[Au(C_6Cl_5)_2]\}_n$ polymer, weak interactions between the Tl atoms and the absorbed VOC molecules modify the emission spectra [8]. On the other hand, emission changes in $[Pt(CN\text{-}R)_4][M(CN)_4]$ (R= *iso*-C_3H_7 or $C_6H_4\text{-}C_nH_{2n+1}$; n=6, 10, 12, 14 and M = Pt, Pd) occur when metal-metal distances are modified due to the presence of VOC molecules in lattice voids [9,10,18]. A related mode of action is operative for supramolecular columns of $Au_3(MeN{=}COMe)_3$ molecules, in which VOCs intercalate or otherwise impact the stacking of one polymorph, thereby altering the emission properties [1–3,19,20]; similarly, crystalline, luminescent $\{Au_3(p\text{-}MeC_6H_4N{=}COEt)_3\}_2$ becomes non-emissive upon exposure to hexafluorobenzene [7].

Among coordination polymers, cyanometallate building blocks have been particularly heavily utilized to form extended networks [21–25]. Despite this, $[Au(CN)_2]^-$ has been relatively neglected as a building block in coordination polymers despite its unusual features: it is linear, forms gold-gold intermolecular interactions, and is luminescent [26–34]. We have reported the new vapochromic $Cu(\mu\text{-}OH_2)_2[Au(CN)_2]_2$ and $Zn[Au(CN)_2]_2$ coordination polymer materials [35–38]. The $Cu(\mu\text{-}OH_2)_2[Au(CN)_2]_2$ system reacts reversibly with certain VOCs containing nitrogen- or oxygen-donors (or irreversibly with NH_3) in the solid-state, generating significant analyte-specific colour changes, as well as distinct changes to the number and position of the ν_{CN} IR bands. An examination of the crystal structures of the dimethylsulfoxide (DMSO), N,N-dimethylformamide (DMF) and pyridine adducts allowed a postulation of the mechanism of reversible vapochromism: the $Cu[Au(CN)_2]_2$ superstructure flexibly distorts to accommodate analyte binding to Cu(II); this binding changes the ligand field, thereby impacting the colour. Changes in the cyanometallate superstructure can also be transmitted via the ν_{CN} pattern [35,36].

Substitution of copper(II) for zinc(II) yields four polymorphs of $Zn[Au(CN)_2]_2$ [37,38], which are highly emissive upon UV-excitation and, more importantly, are extremely sensitive to ammonia vapour; exposure causes a large emission shift [37]. As in the Cu(II) system, ammonia binds to the Zn(II) centre, which triggers the flexible $Zn[Au(CN)_2]_2$ superstructure framework to dynamically adapt to accommodate the analyte. This changes the gold-gold distances in the structure and, since these aurophilic interactions are the source of the emission [30–32], any change in their geometry or topology impacts the emission energy. Both the Cu(II) and Zn(II) coordination polymers are oxygen-stable and thermally robust.

It is clear from the mode of action that the ligand coordination preferences of the metal cation (Cu or Zn) are a key feature influencing which analytes are ultimately sensed, and which are more favoured from a sensitivity perspective [39]. Thus, examining other metal cations as the binding site is worthwhile both as a comparison to the copper(II) and zinc(II) systems and in the possibility of preparing improved sensor materials or a sensor for new analytes that would not be significantly detected by the vapochromic Cu(II) or luminescent Zn(II) cyanoaurate systems.

Towards this end, we recently reported the isostructural $M(\mu\text{-}OH_2)_2[Au(CN)_2]_2$ series, where M = Mn, Fe, Co, Ni and Cu [40,41]. The Cu(II) analogue shows strong, sensitive vapochromic responses to a series of analytes, as described above [35,36]. This manuscript examines the vapochromic response of the isomorphous Co(II) and Ni(II) analogues to a series of analytes—DMF, DMSO and pyridine—which were studied in detail for the Cu(II) system and which showed moderate sensitivity, thereby allowing for a direct comparison of vapochromic efficacy and superstructural flexibility as a function of metal cation. A qualitative report on the vapochromic response of $Co[Au(CN)_2]_2$ with a series of analytes and their IR shifts was very recently reported, but was lacking in any structural or other characterization data on the Co-analyte system or the parent compound [42,43].

2. Experimental Section

2.1. General Procedures

All manipulations were performed in air unless otherwise noted. All reagents were purchased from commercial sources and used as received, except for $M(\mu\text{-}OH_2)[Au(CN)_2]_2$ (M = Co, Ni), which were prepared as previously described [40,41].

CAUTION: Although we have experienced no difficulties, perchlorate salts are potentially explosive and should be used in small quantities and handled with care.

Infrared spectra were recorded on a Thermo Nicolet Nexus 670 FT-IR spectrometer with samples prepared as KBr pressed pellets or analyzed with a Pike Miracol ATR attachment (Table 1). The resolution of the instrument was set at 1 cm^{-1} and the spectra were collected between 400 (KBr) or 700 (ATR) and 4,000 cm^{-1}. Microanalyses (carbon, hydrogen and nitrogen) were performed at Simon Fraser University using a computer-controlled Carlo Erba (Model 1110) CHN analyzer. Thermogravimetric analyses (TGA) of all complexes were performed in an air atmosphere on a Shimadzu TGA-50 instrument at a rate of 5 °C per minute. Solid-state UV-Vis-NIR absorption spectra were measured by reflectance using an Ocean Optics SD2000 spectrophotometer equipped with tungsten halogen and deuterium lamps. Prior to analysis, the samples were ground into fine powders and placed on a glass plate. Magnesium oxide powder, prepared in the same fashion, was used as a reference. Powder X-ray diffractograms were collected on a Rigaku RAXIS-Rapid Auto diffractometer equipped with a Cu K_α source (λ = 1.54056 Å). Samples were mounted on a glass fiber using grease and were exposed, as the phi axis was spinning (10° s^{-1}), for a period of 20 to 60 minutes (with the chi axis fixed at 0 and omega fixed at 90°).

2.2. Synthesis of Zn[Au(CN)$_2$]$_2$(DMSO)$_2$

To a DMSO solution (0.5 mL) of $Zn(ClO_4)_2$ (32 mg, 0.086 mmol), a DMSO solution (0.5 mL) of $K[Au(CN)_2]$ (50 mg, 0.17 mmol) was added dropwise. The solution was allowed to evaporate slowly. Crystals of $Zn[Au(CN)_2]_2(DMSO)_2$ were formed over several days of slow evaporation. Yield: 0.030 g, 42%. Anal. Calcd. for $C_8H_{12}N_4Au_2O_2Zn$: C, 13.35%; H, 7.79%; N, 1.68%. Found: C, 13.50%; H, 8.04%; N, 1.72%. IR (KBr): 3,009 (w), 2,919 (w), 2,186 (m, ν_{CN}), 2,175 (m, ν_{CN}), 1,314 (w), 1,299(w), 1,030 (m), 1,013 (s, $\nu_{S=O}$), 1,005 (s, $\nu_{S=O}$), 957 (m) cm^{-1}.

2.3. Synthesis of Co[Au(CN)$_2$]$_2$(DMSO)$_2$

Co(μ-OH$_2$)$_2$[Au(CN)$_2$]$_2$ (0.125 g, 0.211 mmol) was mixed with DMSO (1 mL) and left to sit for 72 hours, covered. The resulting pink fine powder was then isolated by decantation and left to dry in ambient air. The composition was found to be $Co[Au(CN)_2]_2(DMSO)_2$. Yield: 0.121 g, 80.4%. Anal. Calcd for $C_8H_{12}N_4Au_2CoO_2S_2$: C, 13.47%; H, 1.70%; N, 7.86%. Found: C, 13.51%; H, 1.73%; N, 7.69%. IR (KBr): 3,021(w), 3,009(w), 2,920(w), 2,177(s, ν_{CN}), 1,421(w), 1,408(w), 1,316(w), 1,298(w), 1,031(m), 997(s), 957(m), 938(m), 905(w), 717(w), 467(w), 441(w) cm^{-1}. The same product can also be obtained by vapour absorption of DMSO by Co(μ-OH$_2$)$_2$[Au(CN)$_2$]$_2$ or Co[Au(CN)$_2$]$_2$.

2.4. Synthesis of Ni[Au(CN)$_2$]$_2$(DMSO)$_2$

A DMSO solution (0.75 mL) of $Ni(NO_3)_2{\cdot}6H_2O$ (0.057 g, 0.20 mmol) was added to a DMSO solution (1.75 mL) of $K[Au(CN)_2]$ (0.123 g, 0.427 mmol). A turquoise blue powder started to precipitate after approximately one hour. It was collected by filtration 24 hours later and air-dried. The composition of the final product was determined to be $Ni[Au(CN)_2]_2(DMSO)_2$. Yield: 0.101 g, 70.8%. Anal. Calcd. For $C_8H_{12}N_4Au_2NiO_2S_2$: C, 13.48%; H, 1.70%; N, 7.86%. Found: C, 13.70%; H, 1.81%; N, 8.10%. IR (KBr): 3,434(m), 3,010(w), 2,919(w), 2,189(s, ν_{CN}), 2,180(s, ν_{CN}), 1,629(w), 1,409(w), 1,314(w), 1,299(w), 1,032(m), 1,008(s), 1,001(s), 956(m), 713(w), 480(w), 430(w) cm^{-1}.

2.5. Synthesis of Ni[Au(CN)$_2$]$_2$(DMF)$_2$

Ni(μ-OH$_2$)$_2$[Au(CN)$_2$]$_2$ (0.115 g, 0.194 mmol) was mixed with DMF (1 mL) and left to sit for 24 hours, covered. The resulting blue powder was then isolated by filtration and the composition of the final product was found to be $Ni[Au(CN)_2]_2(DMF)_2$. Yield: 0.092 g, 69%. Anal. Calcd for $C_{10}H_{14}N_6Au_2NiO_2$: C 17.09%, H 2.01%, N 11.96%. Found: C 16.95%, H 2.08%, N 12.24%. IR (KBr): 3,429(m), 2,994(w), 2,964(w), 2933(m), 2,892(w), 2,809(w), 2,189(s, ν_{CN}), 1,658(s), 1,498(w), 1,434(m), 1,418(w), 1,384(m), 1,252(m), 1,109(s), 1,061(m), 689(s), 488(w) cm^{-1}.

2.6. Synthesis of Co[Au(CN)$_2$]$_2$(Pyridine)$_2$

Co(μ-OH$_2$)$_2$[Au(CN)$_2$]$_2$ (0.052 g, 0.088 mmol) was mixed with water/pyridine (2.5 mL, 95:5) and let to sit for 24 hours, covered. The powder became more orange, was isolated by filtration and dried in ambient air. The composition was found to be $Co[Au(CN)_2]_2(pyridine)_2$. Yield: 0.049 g, 78%. Anal. Calcd for $C_{14}H_{10}N_6Au_2Co$: C 23.51%, H 1.41%, N 11.75%. Found: C 23.67%, H 1.55%, N 11.68%. IR

(KBr): 3,086(w), 3,068(w), 3,053(w), 3,024(w), 2,168(s, ν_{CN}), 1,605(s), 1,574(s), 1,486(m), 1,447(s), 1,242(w), 1,216(m), 1,157(w), 1,073(m), 1,041(m), 1,016(w), 946(w), 882(w), 759(m), 698(s), 633(m), 460(w), 431(m) cm^{-1}.

2.7. Synthesis of $Ni[Au(CN)_2]_2(Pyridine)_4$

A 96:4 water/pyridine solution (1.5 mL) of $K[Au(CN)_2]$ (0.059 g, 0.21 mmol) was prepared. This solution was added to a 96:4 water/pyridine solution (1 mL) of $Ni(NO_3)_2 \cdot 6H_2O$ (0.030 g, 0.10 mmol). A purple powder was obtained immediately, which was filtered and air-dried. The product was determined to be $Ni[Au(CN)_2]_2(pyridine)_4$. Yield: 0.070 g, 78%. Anal. Calcd for $C_{24}H_{20}N_8Au_2Ni$: C 33.02%, H 2.31%, N 12.83%. Found: C 32.64%, H 2.25%, N 12.55%. IR (KBr): 3,095(w), 3,070(w), 3,041(w), 3,023(w), 2,993(w), 2,924(w), 2,855(w), 2,171(s, ν_{CN}), 2,143(s, ν_{CN}), 1,602(s), 1,574(m), 1,488(m), 1,449(s), 1,443(s), 1,237(w), 1,216(m), 1,151(w), 1,068(m), 1,042(m), 1,011(w), 769(m), 756(m), 699(s), 631(m), 469(w), 435(m) cm^{-1}.

2.8. Synthesis of $Co[Au(CN)_2]_2$

$Co(\mu\text{-}OH_2)_2[Au(CN)_2]_2$ was heated to 145 °C in an oven for 2 hours to afford cobalt-blue coloured $Co[Au(CN)_2]_2$ quantitatively. The product is stable in air for approximately two days, and was stored under an inert atmosphere to prevent rehydration. Anal. calcd. for $C_4N_4Au_2Co$: C, 8.63%; H, 0%; N, 10.06%. Found: C, 8.51%; H, trace%; N, 9.67%. IR (ATR): 2,177 (s, ν_{CN}), 2,140 cm^{-1} (vw, $^{13}\nu_{CN}$).

2.9. Single Crystal X-Ray Structure of $Zn[Au(CN)_2]_2(DMSO)_2$

A 0.42 × 0.22 × 0.14 mm^3 crystal of $Zn[Au(CN)_2]_2(DMSO)_2$ was mounted on a glass fiber using epoxy adhesive. The data were collected at room temperature on an Enraf Nonius Delft CAD-4 diffractometer with a PMT point detector using the control program DIFRAC [44]. A Mo K_α normal-focus sealed tube operated at 0.736 kW power (46 kV, 16 mA) was utilized for data collection over the range $4° < 2\theta < 60°$. The data was corrected by integration for the effects of absorption using a semi-empirical psi-scan method with a 0.073–0.262 transmission range. Data reduction included corrections for Lorentz and polarization effects using the NRCVAX software suite [45]. Final unit-cell dimensions were determined based on 43 well-centred reflections with a range of $47° < 2\theta < 51°$. The structure of $Zn[Au(CN)_2]_2(DMSO)_2$ was solved in CRYSTALS [46] using direct methods (SIR92) and expanded using Fourier techniques. Diagrams were prepared using ORTEP-3 [47] and POV-Ray [48].

The coordinates and anisotropic temperature factors for all non-hydrogen atoms were refined. The final refinement using observed data ($I_o \geq 2.50\ \sigma(I_o)$) included an extinction parameter, and statistical weights with 177 parameters for 2,953 unique reflections. Hydrogen atoms were placed in calculated positions ($d_{C\text{-}H}$ 0.95 Å) and initially refined with soft restraints on the bond lengths and angles to regularise their geometry; afterwards their coordinate shifts were linked with those of the respective carbon atoms during refinement. Isotropic thermal parameters for the hydrogen atoms were initially assigned proportionately to the equivalent isotropic thermal parameters of their respective carbon atoms. Subsequently the isotropic thermal parameters for the H atoms on the DMSO were constrained

to have identical shifts during refinement. Crystallographic data for $Zn[Au(CN)_2]_2(DMSO)_2$ are tabulated in Table 2. Selected bond lengths and angles are given in Table 3.

2.10. Powder X-Ray Data Indexing/Structure Determination of $M[Au(CN)_2]_2(analyte)_x$ (M = Co and Ni)

The structures of $Ni[Au(CN)_2]_2(DMF)_2$ and $Co[Au(CN)_2]_2(pyridine)_2$ were solved and refined using the DASH software package [49]. After indexing the experimental diffractogram, an automatic background fitting and subtraction was performed, followed by peak fitting to extract the intensity of each peak. To solve the crystal structure, a predefined building block was used. The asymmetric units of $Co[Au(CN)_2]_2(DMF)_2$ [50] and $Cu[Au(CN)_2]_2(pyridine)_2$ [35] were chosen as the building blocks used to solve the structure of $Ni[Au(CN)_2]_2(DMF)_2$ and $Co[Au(CN)_2]_2(pyridine)_2$ respectively. Optimization of the position and orientation of this building block was performed using a simulated annealing algorithm to maximize the agreement with the experimental diffractogram (relative intensity and peak position). The coordinates of each atom in the building blocks were further optimized once a structural model was obtained. The orientation of the pyridine molecules in $Co[Au(CN)_2]_2(pyridine)_2$ was not refined as the diffractogram is mainly affected by the atomic position of the heavy atoms and slight changes in the position of the pyridine molecules do not cause noticeable changes in the diffractogram. The atomic coordinates for $Ni[Au(CN)_2]_2(DMF)_2$ and $Co[Au(CN)_2]_2(pyridine)_2$ are reported in Tables S1 and S2, respectively. Due to the poor quality of the powder diffractogram, the structure of $Ni[Au(CN)_2]_2(DMSO)_2$ could not be determined using DASH. The diffractogram could, however, be indexed using WinPLOTR [51] to a unit cell very similar to that of the analogous Zn-containing polymer. The powder diffractogram for $Co[Au(CN)_2]_2(DMSO)_2$ was also poor and was therefore only indexed with WinPLOTR but not utilized to generate an atomic resolution structure.

3. Results and Discussion

The vapochromic behaviour of the $M(\mu\text{-}OH_2)_2[Au(CN)_2]_2$ (M = Co, Ni) coordination polymers was investigated by exposing them to vapours of DMSO, DMF and pyridine for several hours/days in a sealed container, after which the FT-IR and UV-vis-NIR spectra and the powder X-ray diffractogram of the product were collected. The ν_{CN} bands for each product are reported in Table 1 and compared with those of the product made from solution (see below); visible colour changes were more noticeable for the Co(II) system (Figure 1) than for the Ni(II) analogue. Details for each metal/VOC vapour combination are outlined below.

Table 1. Cyanide vibration frequencies (ν_{CN}, cm^{-1}) for different $M[Au(CN)_2]_2(analyte)_x$ (M = Co, Ni) complexes synthesized from solution and from vapour absorption.

From Solution		From Absorption [a]	
Complex	**ν_{CN} (cm^{-1})**	**Vapour**	**ν_{CN} (cm^{-1})**
$Co(\mu\text{-}OH_2)_2[Au(CN)_2]_2$	2,204(s), 2,168(s)		
$Co[Au(CN)_2]_2(DMSO)_2$	2,177(s)	DMSO	2,176(s)
$Co[Au(CN)_2]_2(DMF)_2$	2,182(s)	DMF	2,182(s)
$Co[Au(CN)_2]_2(pyridine)_x$ [b]	2,168(s)	pyridine	2,168(s), 2,144(s)

Table 1. *Cont.*

From solution		From absorption [a]	
Complex	**ν_{CN}(cm^{-1})**	**Vapour**	**ν_{CN}(cm^{-1})**
Ni(μ-OH$_2$)$_2$[Au(CN)$_2$]$_2$	2,214(s), 2,204(sh), 2,170(s)		
Ni[Au(CN)$_2$]$_2$(DMSO)$_2$	2,189(s), 2,180(s)	DMSO	2,214(m), 2,203(w), 2,181(s), 2,170(s), 2,164(s)
Ni[Au(CN)$_2$]$_2$(DMF)$_2$	2,189(s)	DMF	2,215(m), 2,189(s), 2,171(m)
Ni[Au(CN)$_2$]$_2$(pyridine)$_4$	2,171(s), 2,143(s)	Pyridine	2,213(s), 2,202(m), 2,170(s), 2,162(s), 2,141(s)

[a] Solvent adducts were prepared from Co(μ-OH$_2$)$_2$[Au(CN)$_2$]$_2$ and from Ni(μ-OH$_2$)$_2$[Au(CN)$_2$]$_2$. [b] x = 2 from solution and 4 from absorption methods.

Figure 1. Powders of Co[Au(CN)$_2$]$_2$ (**top left**), Co(μ-OH$_2$)$_2$[Au(CN)$_2$]$_2$ (**top middle**), Co[Au(CN)$_2$]$_2$(pyridine)$_4$ (**top right**), Co[Au(CN)$_2$]$_2$(DMF)$_2$ (**bottom left**) and Co[Au(CN)$_2$]$_2$(DMSO)$_2$ (**bottom right**). The latter three were synthesized by vapour absorption by solid Co[Au(CN)$_2$]$_2$.

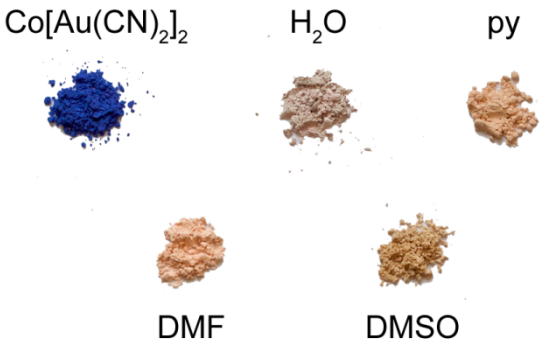

3.1. DMSO-Containing Complexes

Upon exposure to DMSO, the pink Co(μ-OH$_2$)$_2$[Au(CN)$_2$]$_2$ coordination polymer (λ_{max} ≥ 1110, 525 nm) was converted over a three day period to a lighter, brighter pink coloured product (Figure 1; λ_{max} = 1,040, 500, 470 nm) with a ν_{CN} band at 2,176 cm^{-1} (Table 1). This material was stable for months after exposure to ambient atmospheric conditions, indicating that replacement of DMSO molecules for water molecules does not occur at room temperature, which contrasts with the two previously reported Cu[Au(CN)$_2$]$_2$(DMSO)$_2$ polymorphs that readily undergo conversion when exposed to ambient moisture [35]. On the other hand, when Ni(μ-OH$_2$)$_2$[Au(CN)$_2$]$_2$ was exposed to DMSO vapour for one week, ν_{CN} bands attributable to the starting material were still present, as well as new bands at 2,181/2,164 cm^{-1}. No visible colour change occurred.

Since VOC absorption by M(μ-OH$_2$)$_2$[Au(CN)$_2$]$_2$ powders does not lead to single crystals suitable for structural analysis, in order to assist in deciphering the identity and structure of these M[Au(CN)$_2$]$_2$(DMSO)$_x$ products, the preparation of the analogous materials via solution methods was targeted. Thus, the reaction of Co(II), Ni(II) and Zn(II) salts with K[Au(CN)$_2$] in DMSO was conducted; the Zn(II) analogue is included since it is the only one which forms single crystals from DMSO. The Ni and Zn reactions afforded the formation of a blue/turquoise precipitate (Ni) or colourless crystals

(Zn) of $M[Au(CN)_2]_2(DMSO)_2$, determined by elemental analysis. The FT-IR spectra show two strong bands in the cyanide stretching region (ν_{CN} = 2,189/2,180 and 2,186/2,175 cm^{-1} for the Ni and Zn systems, respectively) as well as bands attributable to the sulfoxide (S=O) moiety (1,032–956 cm^{-1}) [52]. The slight shift in ν_{CN} between the Ni and Zn materials can be attributed to the different transition metal bound to the nitrogen atom of each cyanide group [53].

The $Zn[Au(CN)_2]_2(DMSO)_2$ structure (Figure 2, Tables 2 and 3) contains a single octahedral Zn(II) centre, with two *cis*-coordinated oxygen-bound DMSO molecules (Figure 2(a), Zn-O = 2.120(6) and 2.075(6) Å). The remaining four sites around the Zn(II) are coordinated with $[Au(CN)_2]^-$ units with an average Zn-N bond length of 2.144(8) Å, longer than the <2.0 Å Zn-N bond lengths in the tetrahedrally coordinated polymorphs of $Zn[Au(CN)_2]_2$ [37,38]. A 2-D corrugated structure, with DMSO molecules protruding from the apex of the corrugation, is formed by the bridging $[Au(CN)_2]^-$ units (Figure 2(c)). The closest contact between sheets is a Au-Au interaction of 3.4943(6) Å. A similar crystal structure was observed for the Cu(II) system [35].

Table 2. Crystallographic data for $Zn[Au(CN)_2]_2(DMSO)_2$.

Formula	$C_8H_{12}N_4Au_2O_2S_2Zn$
Formula weight, M_r	719.66
Colour	colourless
Shape	chunk
Dimensions, mm^3	0.14 × 0.22 × 0.42
Crystal system	monoclinic
Space group	$P2_1/c$
Z	4
T, K	293
a, Å	7.8403(11)
b, Å	12.8395(12)
c, Å	16.4572(17)
β, deg	98.891(10)
Volume, $Å^3$	1636.8(3)
D_{calcd}, g/cm^3	2.920
λ, nm (Mo K_α)	0.71073
2θ range, deg	4–60
μ, mm^{-1}	19.592
Reflns, total	5010
Reflns, unique	4801
Reflns, $I_o \geq 2.50\ \sigma(I_o)$	2953
Extinction coefficient	16.0(15)
R (F_o)	0.0342
wR (F_o)	0.0396

Figure 2. Extended 2-D structure of $Zn[Au(CN)_2]_2(DMSO)_2$. (**a**) Local geometry of Zn, showing thermal ellipsoids; (**b**) A single 2-D sheet, viewed down the face of the sheet; (**c**) A pair of 2-D sheets, viewed perpendicular to the sheet face, long Au(1)-Au(2*) interactions 3.4943(6) Å represents the closest contact between sheets (DMSO molecules excluded for clarity).

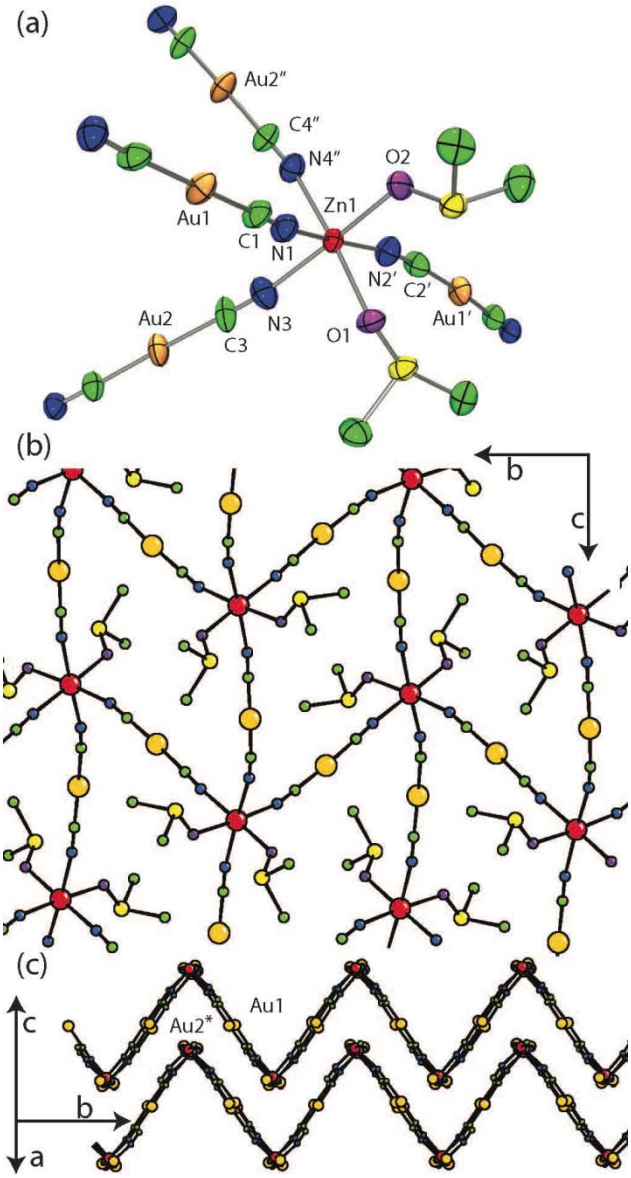

Table 3. Selected bond lengths (Å) and angles (deg) for $Zn[Au(CN)_2]_2(DMSO)_2$ [a].

Zn(1)–N(1)	2.163(7)	Zn(1)–N(2')	2.167(8)
Zn(1)–N(3)	2.140(8)	Zn(1)–N(4")	2.104(8)
Zn(1)–O(1)	2.120(6)	Zn(1)–O(2)	2.075(6)
Au(1)–Au(2*)	3.4943(6)		
N(2')–Zn(1)–N(4")	91.3(3)	N(2')–Zn(1)–O(1)	88.8(3)
N(4")–Zn(1)–O(1)	175.7(3)	N(2')–Zn(1)–O(2)	88.3(3)
N(4")–Zn(1)–O(2)	91.2(3)	O(1)–Zn(1)–O(2)	93.2(3)
N(2')–Zn(1)–N(1)	172.5(3)	N(4")–Zn(1)–N(1)	93.0(3)

Table 3. *Cont.*

O(1)–Zn(1)–N(1)	87.4(3)	O(2)–Zn(1)–N(1)	85.4(3)
N(2')–Zn(1)–N(3)	94.1(3)	N(4'')–Zn(1)–N(3)	87.9(3)
O(1)–Zn(1)–N(3)	87.8(3)	O(2)–Zn(1)–N(3)	177.4(3)
N(1)–Zn(1)–N(3)	92.3(3)	Zn(1)–O(1)–S(1)	126.3(4)
Zn(1)–O(2)–S(2)	126.0(4)	Zn(1)–N(1)–C(1)	172.8(8)
Zn(1')–N(2')–C(2')	169.4(8)	Zn(1)–N(3)–C(3)	172.8(10)
Zn(1)–N(4'')–C(4'')	167.3(8)	Au(2*)–Au(1)–C(1)	105.3(3)

[a] Symmetry operations: ' = x − 1, −y + 3/2, z − ½; '' = −x + 4, y − 1/2, −z + 1/2; * = −x + 4, −y + 2, −z + 1.

Although no single crystal of $Ni[Au(CN)_2]_2(DMSO)_2$ suitable for X-ray crystallography could be obtained, its powder X-ray diffractogram showed similar features to the diffractograms of the $Zn[Au(CN)_2]_2(DMSO)_2$ and $Cu[Au(CN)_2]_2(DMSO)_2$ (blue polymorph) coordination polymers (Figure 3) [35]. The diffractogram of $Ni[Au(CN)_2]_2(DMSO)_2$ could be indexed to a monoclinic unit cell, with parameters very similar to those of the Zn analogue (Table 4). Thus, the structure of $Ni[Au(CN)_2]_2(DMSO)_2$ likely consists of octahedral Ni(II) ions coordinated by two DMSO molecules in a *cis* fashion and connected to four other Ni(II) centres via $[Au(CN)_2]^-$ units, generating corrugated 2-D sheets; due to the poor quality of the diffractogram, no effort was made to structurally model the data any further. Note that the ν_{CN} data and powder X-ray diffractograms for $Ni[Au(CN)_2]_2(DMSO)_2$ do not perfectly match those obtained via vapour absorption of DMSO by $Ni(\mu\text{-}OH_2)_2[Au(CN)_2]_2$, indicating that a related, but different structure is likely accessed by vapour absorption.

Figure 3. Comparison between the powder X-ray diffractograms predicted for $Zn[Au(CN)_2]_2(DMSO)_2$ (Zn, green) and the blue $Cu[Au(CN)_2]_2(DMSO)_2$ polymorph (Cu, blue), with the diffractogram obtained experimentally for $Ni[Au(CN)_2]_2(DMSO)_2$ (Ni, orange), prepared via solution methods.

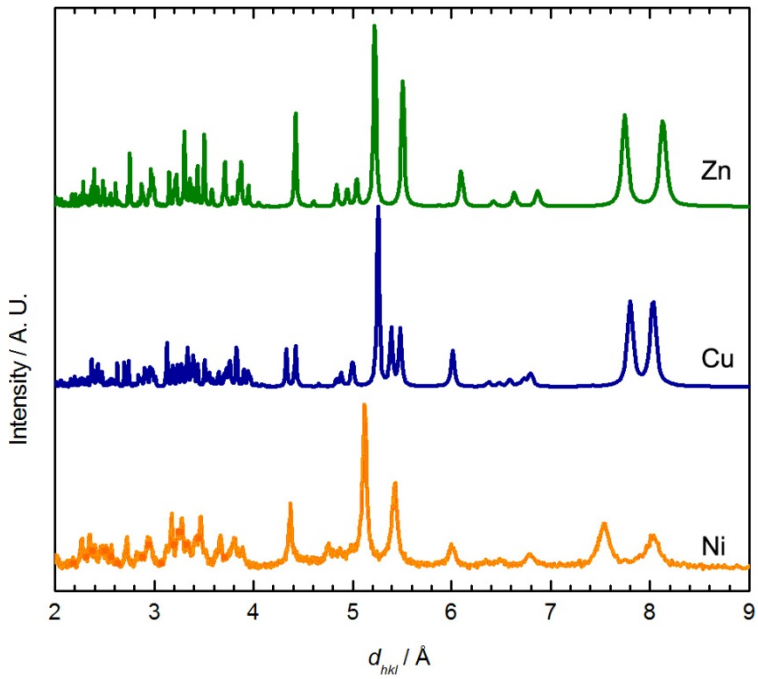

Table 4. Unit cell parameters determined for the $M[Au(CN)_2]_2(DMSO)_2$ coordination polymers (M = Zn, Cu (blue polymorph), Ni and Co), by either single crystal or powder X-ray diffraction.

	Zn	Cu (Blue)	Ni	Co
Sample	**Crystal**	**Crystal**	**Powder**	**Powder**
crystal system	monoclinic	triclinic	monoclinic	monoclinic
space group	P21/c	P-1	$P2_1/c$	C2/m
a, Å	7.8403(11)	7.874(7)	7.63	6.35
b, Å	12.8395(12)	12.761(11)	12.84	14.80
c, Å	16.4572(17)	16.207(13)	16.30	7.35
α, deg	90.0	89.61(7)	90.0	90.0
β, deg	98.891(10)	82.29(7)	98.89	100.77
γ, deg	90.0	88.57(7)	90.0	90.0
Volume, $Å^3$	1,636.77	1,613.2(24)	1,577.65	677.52

Although the analogous reaction between a Co(II) salt and $K[Au(CN)_2]$ in neat DMSO yielded an inseparable mixture of products, when pink $Co(\mu\text{-}OH_2)_2[Au(CN)_2]_2$ was immersed in DMSO for three days, a slight colour change occurred. The resulting light pink powder was isolated and the chemical composition was determined to be $Co[Au(CN)_2]_2(DMSO)_2$. The FT-IR spectrum of this product contains only one ν_{CN} band (2,176 cm^{-1}), analogous to that observed by vapour absorption (Table 1).

This reaction did not yield single crystals suitable for X-ray analysis, only microcrystalline powder. The powder diffractogram (Figure 4) was indexed and the unit cell parameters obtained are reported in Table 4. The diffractogram and the unit cell parameters do not match that of the Zn, Cu or Ni-containing $M[Au(CN)_2]_2(DMSO)_2$ polymers (Figure 3 and Table 4), which suggests that a different structural arrangement is adopted. Due to the poor quality of the diffractogram, no structure refinement could be performed, but a structural model is proposed based on comparisons with other known complexes.

Figure 4. Comparison between the powder X-ray diffractogram determined experimentally for the $Co[Au(CN)_2]_2(DMSO)_2$ (Co, purple) and the diffractogram predicted for $Mn[Au(CN)_2]_2(H_2O)_2$ from the single crystal structure (Mn, blue) [54].

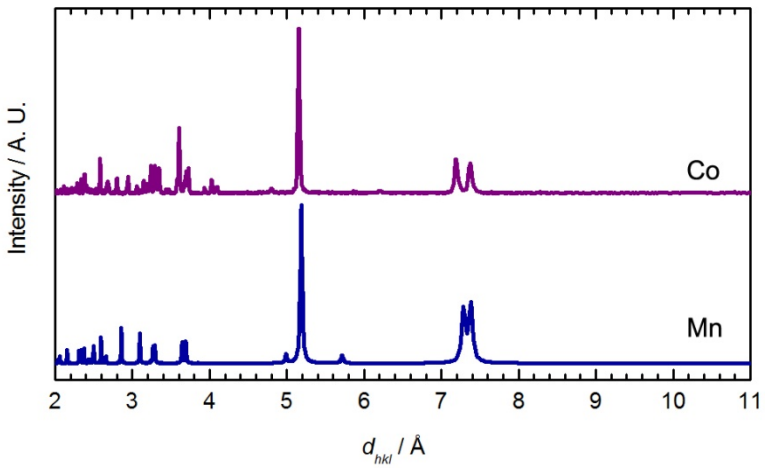

The presence of only one ν_{CN} band, shifted from free $[Au(CN)_2]^-$, suggests that all the cyanide groups are in a similar environment and N-bound to Co(II). This could be the case if the structure of $Co[Au(CN)_2]_2(DMSO)_2$ contained square-grid arrays of $Co[Au(CN)_2]_2$ with DMSO molecules bound to Co(II) ions in a *trans* fashion, on each side of the grid. This type of structure has been observed for the previously reported $Co[Au(CN)_2]_2(DMF)_2$ [50] and $Mn[Au(CN)_2]_2(H_2O)_2$ [54] coordination polymers. Although the ν_{CN} band observed for $Co[Au(CN)_2]_2(DMSO)_2$ (2,176 cm^{-1}) is similar to that for the DMF analogue (2,179 cm^{-1}) [35], the powder diffractograms are a poor match.

The main features in the diffractograms of $Co[Au(CN)_2]_2(DMSO)_2$ and $Mn[Au(CN)_2]_2(H_2O)_2$ [54] are similar (Figure 4). The packing in $Co[Au(CN)_2]_2(DMF)_2$ differs from $Mn[Au(CN)_2]_2(H_2O)_2$ since the $Co[Au(CN)_2]_2$ layers stack in discrete pairs whereas the $Mn[Au(CN)_2]_2$ layers are equally spaced and do not form pairs of layers. It is hence suggested that, analogous to the $Mn[Au(CN)_2]_2(H_2O)_2$ superstructure, the $Co[Au(CN)_2]_2(DMSO)_2$ polymer contains flat and equally spaced square-grid arrays, with DMSO molecules bound in a *trans* fashion.

With this information in hand, it is clear that vapour absorption of DMSO by $Co(\mu\text{-}OH_2)_2[Au(CN)_2]_2$ gives $Co[Au(CN)_2]_2(DMSO)_2$ cleanly; the solution method yields a product with comparable UV-vis, powder X-ray and IR data. However, the Ni(II) system does not run to completion, even after a week of vapour exposure, and the products from vapour and solution methods, although related, do not appear to be identical.

3.2. DMF-Containing Complexes

When $Co(\mu\text{-}OH_2)_2[Au(CN)_2]_2$ was exposed to DMF vapour, faint colour changes to a light, bright pink (λ_{max} = 1035, 490, 468 nm) were observed after several hours (Figure 1), and the IR spectrum indicated a clean conversion; a single ν_{CN} peak at 2,182 cm^{-1} was generated (Table 1). The analogous solution-based synthetic product has a comparable FTIR spectrum and powder X-ray diffractogram to that obtained by vapour absorption, both of which are indistinguishable from that of the previously published $Co[Au(CN)_2]_2(DMF)_2$ system (Figure 5) [50]; this is therefore the product that is obtained. For the Ni(II) analogue, after one week of being exposed to DMF vapour, the FT-IR spectrum of the product showed the presence of the starting $Ni(\mu\text{-}OH_2)_2[Au(CN)_2]_2$ compound as well as an additional band at 2,184 cm^{-1}; no significant colour change was observed.

For comparison, when $Ni(\mu\text{-}OH_2)_2[Au(CN)_2]_2$ was immersed in DMF for one day, a colour change from light green to blue was observed, similar to $Co[Au(CN)_2]_2(DMF)_2$. The FT-IR spectrum of the isolated product showed only one ν_{CN} band at 2,189 cm^{-1}. The chemical composition was determined to be $Ni[Au(CN)_2]_2(DMF)_2$ from elemental analysis, comparable to the previously reported $Co[Au(CN)_2]_2(DMF)_2$ coordination polymer [50] but different from that of the Cu(II)-containing analogue, in which only one DMF molecule was incorporated. The unit cell obtained from indexing the powder X-ray diffractogram of $Ni[Au(CN)_2]_2(DMF)_2$ (Figure 5-Ni) is also similar to that of $Co[Au(CN)_2]_2(DMF)_2$ (Table 5) [50].

Figure 5. Comparison between the powder X-ray diffractogram (generated from single-crystal data) for $Co[Au(CN)_2]_2(DMF)_2$ (Co, purple) [50], the experimental diffractogram for $Ni[Au(CN)_2]_2(DMF)_2$ (Ni, orange) and the diffractogram predicted by the proposed structural model (Ni*, black).

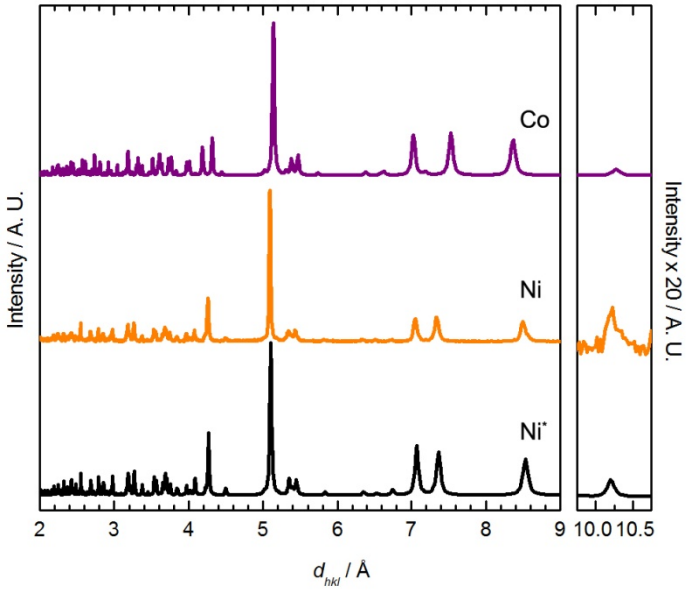

Table 5. Unit cell parameters determined for the $M[Au(CN)_2]_2(DMF)_2$ (M = Co, Ni) and $Co[Au(CN)_2]_2(pyridine)_2$ coordination polymers by either single crystal or powder X-ray diffraction.

	$Co[Au(CN)_2]_2(DMF)_2$	**$Ni[Au(CN)_2]_2(DMF)_2$**	**$Co[Au(CN)_2]_2(pyridine)_2$**
Sample	**Crystal[32]**	**Powder**	**Powder**
crystal system	monoclinic	monoclinic	monoclinic
space group	$P2_1/c$	$P2_1/c$	P21/c
a, Å	8.375(2)	8.5659	8.9334
b, Å	14.054(5)	14.1445	14.0712
c, Å	15.077(4)	14.7907	15.0425
α, deg	90.0	90.0	90.0
β, deg	92.75(2)	95.011	99.2538
γ, deg	90.0	90.0	90.0
Volume, $Å^3$	1,772.6(9)	1785.2	1,866.3

Using the atomic coordinates of the published Co(II) analogue as a starting point, the structure of $Ni[Au(CN)_2]_2(DMF)_2$ was determined from the observed powder X-ray diffractogram (the atomic coordinates are reported in Table S1). Figure 6 shows the proposed model for $Ni[Au(CN)_2]_2(DMF)_2$.

As with $Co[Au(CN)_2]_2(DMF)_2$, the structure contains 2-D square grids of $Ni[Au(CN)_2]_2$ (Figure 6(A)). The DMF molecules are O-bound to the Ni(II) centres on each side of the grids, which stack in an offset manner to accommodate the DMF molecules. The $[Au(CN)_2]^-$ units are slightly bent and sit above and below the plane containing the Ni(II) centres (Figure 6(B,C)). As observed in the $Co[Au(CN)_2]_2(DMF)_2$ structure, the layers stack in discrete pairs with aurophilic interactions of *ca.* 3.3 Å forming the pair, whereas Au-Au distances of *ca.* 5.4 Å separate each pair of layers.

Figure 6. Structural model proposed for $Ni[Au(CN)_2]_2(DMF)_2$: (**A**). A 2-D square grid array with DMF molecules coordinated on both sides of the $Ni[Au(CN)_2]_2$ layer; (**B**) and (**C**). Side-view of a layer showing the relative position of the $[Au(CN)_2]^-$ units with respect to the Ni(II) centres.

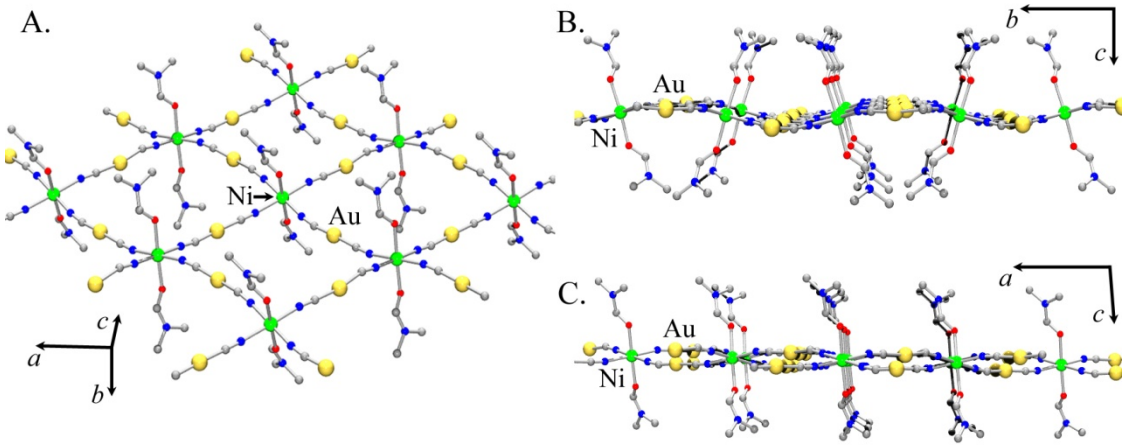

Thus, both Co(II) and Ni(II) analogues of $M(\mu\text{-}OH_2)_2[Au(CN)_2]_2$ sense DMF as an analyte, although the Co(II) system reacts more cleanly and quickly. Both form similar 2-D layer structures of $M[Au(CN)_2]_2(DMF)_2$, with the same product being generated from solution or vapour absorption. However, the Ni(II) analogue only partially converts to product in the vapour absorption experiment, and as a result the expected visible vapochromism (green to blue by solution methods) was not observed; this putative vapochromic response was likely attenuated by the residual absorption bands of the unreacted starting material.

3.3. Pyridine-Containing Complexes

When $Co(\mu\text{-}OH_2)_2[Au(CN)_2]_2$ was exposed to pyridine vapour, conversion to a light pink product (λ_{max} = 1,000, 525, 485 nm, Figure 1) having ν_{CN} bands at 2,168/2,144 cm^{-1} occurred (Table 1). Upon exposure to pyridine vapour, $Ni(\mu\text{-}OH_2)_2[Au(CN)_2]_2$ undergoes a colour change, from light green to blue over several days. The FT-IR spectrum shows ν_{CN} bands of the starting material and additional bands at 2,170/2,162/2,141 cm^{-1}; this complexity likely indicates the formation of a mixture of analyte-containing products.

On the solution synthesis side, when a powdered sample of $Co(\mu\text{-}OH_2)_2[Au(CN)_2]_2$ was immersed for one day in a mixture of water and pyridine (96:4), a slight colour change was observed. The FT-IR spectrum of the isolated powder showed only one strong ν_{CN} band at 2,168 cm^{-1} (Table 1), reminiscent of that of the $Co[Au(CN)_2]_2(DMF)_2$ system. Thus, a different product is obtained in solution. Pyridine-based bands could also be observed.

The powder X-ray diffractogram of the solution-based product, which analyzes as $Co[Au(CN)_2]_2(pyridine)_2$, is shown in Figure 7 and is different than the material obtained by vapour diffusion; it also shows similar features to the diffractogram of $Co[Au(CN)_2]_2(DMF)_2$ (Figure 5) and $Cu[Au(CN)_2]_2(pyridine)_2$. The diffractogram was indexed and the optimized unit cell parameters are reported in Table 5. They are comparable with those of the Ni and Co-containing $M[Au(CN)_2]_2(DMF)_2$ complexes (Figure 6).

Figure 7. Comparison between the powder X-ray diffractogram (generated from single-crystal data) for $Cu[Au(CN)_2]_2(pyridine)_2$ (Cu, orange) [35], the experimental diffractogram of $Co[Au(CN)_2]_2(pyridine)_2$ (Co, purple), and the diffractogram predicted by its structural model (Co*, black).

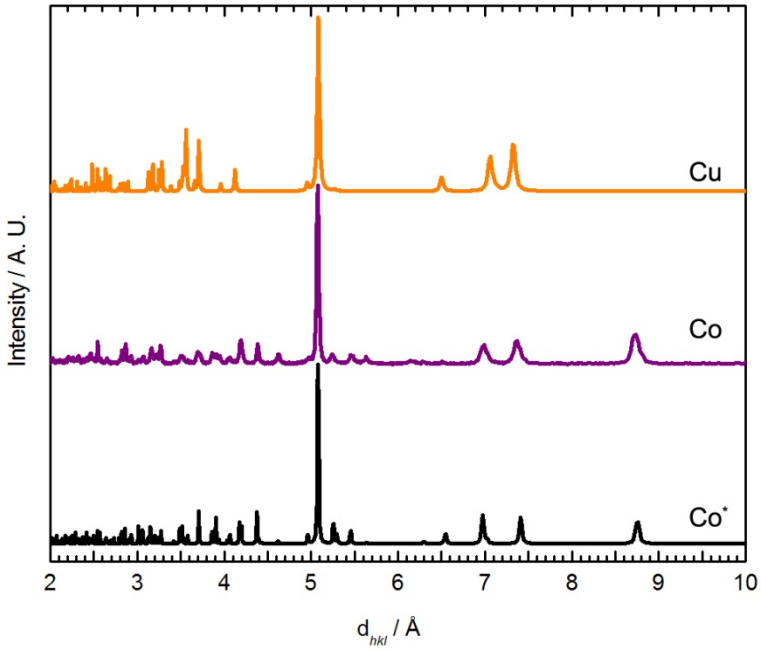

Figure 8. Structural model proposed for $Co[Au(CN)_2]_2(pyridine)_2$: (**A**) 2-D square-grid array with pyridine molecules on both sides of the grid; (**B**) Side-view of a 2-D layer, showing the position of the $[Au(CN)_2]^-$ units with respect to the Co(II) centres.

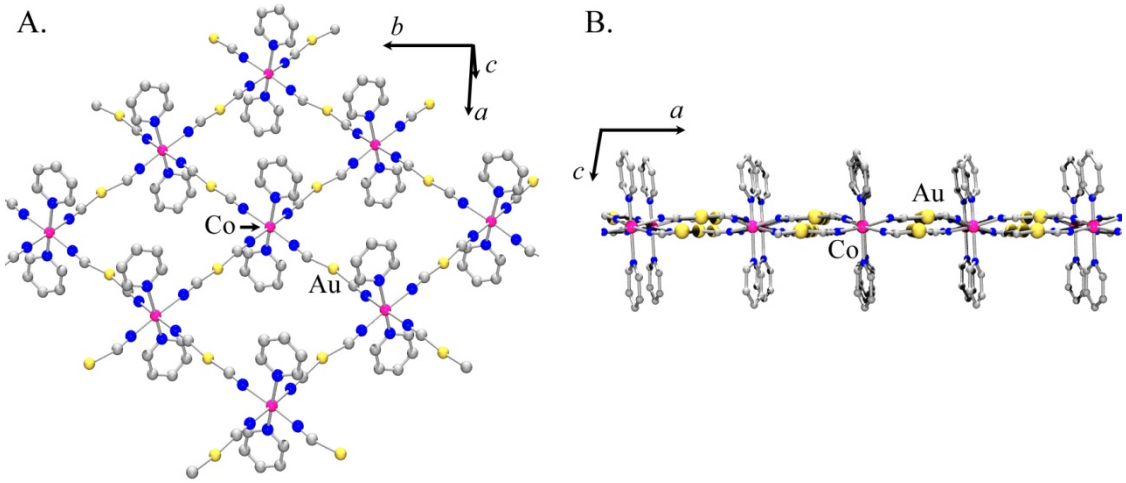

Using a combination of the $Cu[Au(CN)_2]_2(pyridine)_2$ and $Co[Au(CN)_2]_2(DMF)_2$ structures as a starting point, a structural model is proposed for $Co[Au(CN)_2]_2(pyridine)_2$ (the corresponding atomic coordinates are reported in Table S2). The structure consists of 2-D square grids of $Co[Au(CN)_2]_2$ with pyridine molecules N-bound to the Co(II) centres on both sides of the layer (Figure 8(A)). The structure differs from the Cu(II) analogue as all the cyanide groups are equidistant from the Co(II) centres and no Jahn-Teller distortion is observed. Also, the $Co[Au(CN)_2]_2$ layers are not completely flat as in the $Cu[Au(CN)_2]_2$ system, but the $[Au(CN)_2]^-$ units are buckled in an alternate way on each

side of the layer (Figure 8(B)), as is observed in the related $Co[Au(CN)_2]_2(DMF)_2$ polymer [50]. This arrangement allows π–π interactions between the pyridine rings, but no aurophilic interactions are present as the closest contact between two Au atoms is approx. 3.7 Å. The powder diffractogram predicted by this model is compared to the experimental diffractogram of $Co[Au(CN)_2]_2(pyridine)_2$ in Figure 7.

The addition of $Ni(NO_3)_2{\cdot}6H_2O$ to $KAu(CN)_2$ in a mixture of water and pyridine (96:4) generated purple $Ni[Au(CN)_2]_2(pyridine)_4$, confirmed by elemental analysis. The FT-IR spectrum of this product shows two ν_{CN} bands (2,171 and 2,143 cm^{-1}), consistent with two of the three bands observed by vapour diffusion. Depending on the reaction conditions, variable amounts of an uncharacterized material could also be generated (as indicated by IR: 2182, 2153 cm^{-1}) but a pure sample could not be isolated.

Clearly, pyridine as an analyte yields the most complex, least clean conversions for both Co(II) and Ni(II) analogues. Thus, for Co(II), a bis-pyridine adduct forms from aqueous pyridine solution, while vapour absorption methods generated a different product. A $Ni[Au(CN)_2]_2(pyridine)_4$ complex was isolated via solution methods, confirmed by elemental analysis. The powder X-ray diffractograms of $Ni[Au(CN)_2]_2(pyridine)_4$ and the Co vapochromic product are very similar, which suggests that the product of pyridine vapour with the Co(II) system is a tetrakis-pyridine adduct. Finally, pyridine vapour absorption by $Ni(\mu\text{-}OH_2)_2[Au(CN)_2]_2$ is the least clean of all the reactions studied herein, generating $Ni[Au(CN)_2]_2(pyridine)_4$, another unidentified product (perhaps a bis-pyridine adduct) as well as leaving residual starting material.

3.4. Analyte-Free $M[Au(CN)_2]_2$ Systems

Analyte-free systems were investigated in order to see if the vapochromic response would be improved without the presence of an initial analyte molecule (H_2O) in the structure. $Co[Au(CN)_2]_2$ was synthesized by heating $Co(\mu\text{-}OH_2)_2[Au(CN)_2]_2$ to at least 110 °C for a minimum of one hour (ideally, 145 °C for two hours; heating at 180 °C for 10 minutes was very recently reported as an alternative synthesis [42]). The compound changes from a light pink colour (octahedral Co(II)) to an intense cobalt-blue colour (tetrahedral Co(II)). $Co[Au(CN)_2]_2$ is stable in ambient air for approximately two days, whereupon it rehydrates to a compound with a similar powder X-ray diffractogram and IR spectrum to $Co(\mu\text{-}OH_2)_2[Au(CN)_2]_2$, but is a light purple colour; its identity is under investigation.

The structure of $Co[Au(CN)_2]_2$ was deduced by matching the powder X-ray diffractogram to that of the isostructural compound [37], γ-$Zn[Au(CN)_2]_2$ (Figure S1), indexing the data accordingly (spacegroup *P*-4*b*2, a = 6.7968(17) Å, c = 8.4651(3) Å) and refining atomic positions (Tables S3 and S4). The cobalt(II) centres are tetrahedrally coordinated through the nitrogen end of four $[Au(CN)_2]^-$ units, creating a tetragonal diamond-type lattice (Figure 9). There are four interpenetrated networks that are linked together via aurophilic interactions (3.33 and 3.56 Å). Note that a previously reported synthesis of $Co[Au(CN)_2]_2$ (by a simple addition of salt [55]) generated a different polymorph (equivalent to quartz-type α-$Zn[Au(CN)_2]_2$) [37,38], while using another route, via solvent-free grinding of $Co(OH_2)_2[Au(CN)_2]_2$, the structure was not determined [42].

Figure 9. Extended 3-D structure of $Co[Au(CN)_2]_2$, looking down the *c* axis. Dashed lines represent Au-Au interactions.

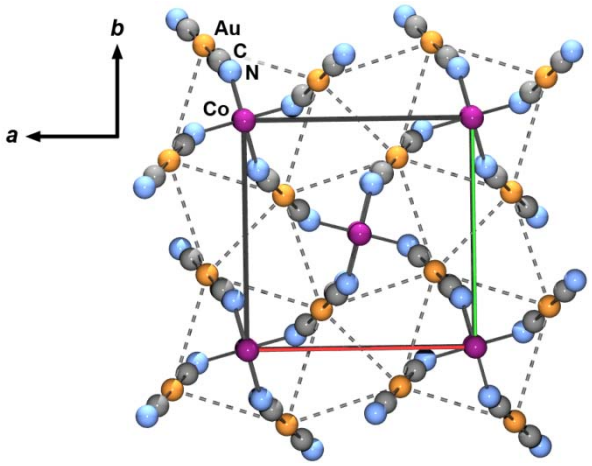

Vapochromic experiments were also performed on $Co[Au(CN)_2]_2$ with DMF, DMSO, and pyridine as analytes. Uptake occurred in all cases, yielding $Co[Au(CN)_2]_2(analyte)_x$ materials in similar shades of light pink; with DMF as the analyte, the complex showed the fastest conversion (about 1 day), whereas pyridine showed the slowest conversion (several days). Based on IR and powder X-ray diffraction data, the complexes that form using DMF and DMSO are identical to those produced from vapour absorption by $Co(\mu\text{-}OH_2)_2[Au(CN)_2]_2$. The complex with pyridine shows two ν_{CN} bands at 2,170 and 2,142 cm^{-1} and a powder X-ray diffractogram matching the $Co[Au(CN)_2]_2(pyridine)_4$ adduct identified via vapour absorption by $Co(\mu\text{-}OH_2)_2[Au(CN)_2]_2$, rather than the bis-pyridine adduct obtained by solution methods. These IR spectroscopic results broadly match those very recently reported for the addition of a range of donor solvents (including pyridine, DMSO and DMF, as reported here) to $Co[Au(CN)_2]_2$ [42].

The synthesis of $Ni[Au(CN)_2]_2$ was attempted by several methods but the desired product could not be obtained. Since the dehydration temperature for $Ni(\mu\text{-}OH_2)_2[Au(CN)_2]_2$ is between 215–260 °C, it is necessary to heat above 260 °C for extended periods of time to dehydrate it, but doing so resulted in decomposition. Attempts to effect chemical dehydration by stirring $Ni(\mu\text{-}OH_2)_2[Au(CN)_2]_2$ in glacial acetic acid or refluxing in trimethylsilylchloride resulted in no change. The addition of $[^nBu_4N][Au(CN)_2]$ [56] to anhydrous $NiCl_2$·DME in dry organic solvents under an inert, dry atmosphere yielded other products which are under investigation [57], but did not generate $Ni[Au(CN)_2]_2$. It therefore appears that $Ni(\mu\text{-}OH_2)_2[Au(CN)_2]_2$ is exceptionally stable, which is in agreement with the vapour absorption results, which indicate only partial conversion in every case.

3.5. Comparison of M[Au(CN)$_2$]$_2$-Based Vapochromic Materials (M = Co, Ni, Cu)

The $M[Au(CN)_2]_2(analyte)_x$ polymers show visible vapochromism since each analyte molecule that is incorporated binds to the M(II) centre and modifies differently its crystal field splitting. As a consequence, the colours of the vapochromic compounds change as the *d–d* absorbance bands shift [35,36]. Table 6 shows the solid-state UV-vis-NIR absorbance maxima for the analyte-containing compounds prepared from solution (*vs.* direct analyte absorption by the solid).

Table 6. Absorbance maxima ($\lambda_{max\ abs}$, nm) observed in the solid-state UV-Vis-NIR absorbance spectra of the $M[Au(CN)_2]_2(analyte)_x$ (M = Co, Ni) coordination polymers prepared from solution.

Ni(II) complexes	**$\lambda_{max\ abs}$ (nm)**		
$Ni(\mu\text{-}OH_2)_2[Au(CN)_2]_2$	930	625	390
$Ni[Au(CN)_2]_2(DMSO)_2$	925	620	385
$Ni[Au(CN)_2]_2(DMF)_2$	925	610	385
$Ni[Au(CN)_2]_2(pyridine)_4$	905	575	375
Co(II) complexes			
$Co(\mu\text{-}OH_2)_2[Au(CN)_2]_2$	>1,110	525	
$Co[Au(CN)_2]_2(DMSO)_2$	1,040	500	470
$Co[Au(CN)_2]_2(DMF)_2$	1,035	490	468
$Co[Au(CN)_2]_2(pyridine)_2$	1,000	525(sh)	485
$Co[Au(CN)_2]_2$	590	550 (sh)	365

The data in Table 6 and Figure 1 suggests that identification of the different $M[Au(CN)_2]_2(analyte)_2$ polymers (M = Co, Ni) purely on the basis of colour cannot be accomplished as easily as for the Cu(II)-based analogues [35,36]. The M(II) coordination sphere in the $M[Au(CN)_2]_2(analyte)_2$ polymers is very similar: an octahedral geometry with four cyanide groups occupying the same plane. The only difference lies in the two donor analytes that are *trans* to each other ($M(NC)_4(O\text{-ligand})_2$ *vs.* $M(NC)_4(N\text{-ligand})_2$). As a result, the crystal field splitting of the M(II) centres in each $M[Au(CN)_2]_2(analyte)_2$ is very similar and, hence, so is their colour, particularly for DMSO and DMF analytes; some differentiation for pyridine is possible. The spectra of the $M(\mu\text{-}OH_2)_2[Au(CN)_2]_2$ polymers containing $M(NC)_2(O\text{-ligand})_4$ centres is, however, shifted to slightly lower energy. The analyte-free $Co[Au(CN)_2]_2$ system is also markedly different from all Co(II)-analyte adducts, consistent with tetrahedral *vs.* octahedral Co(II) centres.

Upon comparing the reactivity of the $M[Au(CN)_2]_2$-based systems, analyte exchange is quickest for M = Cu(II) and Zn(II) [35–38], followed by the Co(II) system and least so in the Ni(II) system, for which analyte exchange was found to be only partial, with a mixture of products obtained; this is likely due to the relative kinetic inertness of Ni(II) complexes. Thus, the Ni(II)-systems are not likely to be very useful vapochromic materials for VOC sensing. Indeed, the most easily visible vapochromic system reported here is the analyte-free $Co[Au(CN)_2]_2$, for which drastic colour changes upon analyte-binding occurs, but differentiation of the products obtained with different analytes is more difficult. Note that other factors, such as particle size/surface area and analyte vapour pressure, also influence the overall kinetic response of the material.

From a structural perspective, it is known that a system does not need to be porous in order to undergo guest uptake [58]. For example, a flexible metal-ligand superstructure can dynamically adapt in order to accommodate a variety of potential guests, as is the case here [58–64]. Despite the range of analyte molecules utilized, the basic structural motif of the $M[Au(CN)_2]_2(analyte)_x$ coordination polymers remained the same in most cases: a 2-D square-grid $M[Au(CN)_2]_2$ network was the basic structural feature, which is flexible and can adapt to accommodate the requisite structural changes, depending on the metal ion and analyte type. Scheme 1 summarizes the different types of structural distortions observed for the $M[Au(CN)_2]_2$-based systems (M = Co, Ni, Cu).

Scheme 1. Different structural models observed for the $M[Au(CN)_2]_2(analyte)_x$ polymers, all resulting from the structural flexibility of the basic $M[Au(CN)_2]_2$ square-grid array.

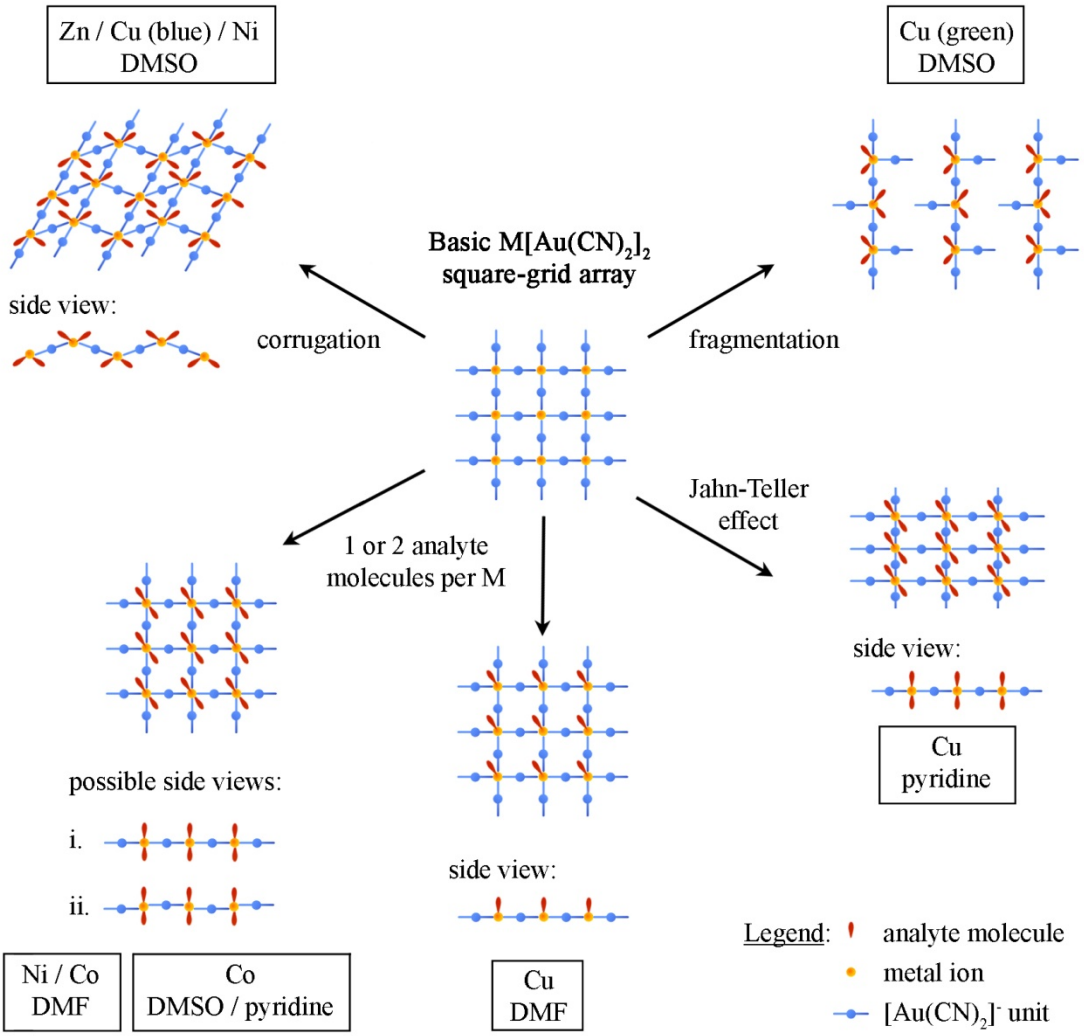

The major mode of flexibility [62–64] lies in the fact that the 2-D square-grid can be entirely flat, as in the $M[Au(CN)_2]_2(DMF)_2$ or $M[Au(CN)_2]_2(pyridine)_2$ complexes, or it can buckle to generate a corrugated 2-D array, as observed in several $M[Au(CN)_2]_2(DMSO)_2$ (M = Zn, Ni or Cu (blue polymorph)) polymers. In addition, in a flat square-grid, the $[Au(CN)_2]^-$ units can lie completely co-planar with the M(II) centres as in $Cu[Au(CN)_2]_2(pyridine)_2$ or bent out of the M(II)-containing plane, as in $M[Au(CN)_2]_2(DMF)_2$. For a given analyte, similar structures are usually observed despite the change in metal centre. DMSO is the only type of guest utilized that forces corrugation of the layers, whereas DMF and pyridine favour flat square-grid arrays to be obtained.

Due to Jahn-Teller distortions, the structures of the polymers containing Cu(II) ions are more axially elongated than that of the Ni(II) and Co(II)-containing polymers. This form of structural flexibility is particularly important since substantially different FT-IR signatures in the cyanide vibration region for the Cu(II)-analogues are generated depending on the axial/equatorial cyanide bonding arrangement in the system; this detection methodology is less striking for the Co/Ni analogues, which don't have the same geometric flexibility as Cu(II) [35]. In the $Cu[Au(CN)_2]_2(analyte)_2$ system, the differences in cyanide vibration frequency between certain analyte adducts vary by up to 70 cm^{-1}. However, the

differentiation between DMF, DMSO, and pyridine analytes in the Co(II) analogue is poorer due to similar colour and ν_{CN} frequencies. The FT-IR signatures in the cyanide vibration region for the $Ni[Au(CN)_2]_2(analyte)_x$ polymers, on the other hand, are different from each other, allowing for analyte identification if analyte exchange actually occurs.

4. Conclusions

In summary, the $Co[Au(CN)_2]_2$-based systems react when exposed to different analytes, but detection and identification of the analyte by FT-IR and UV-vis spectroscopies are more difficult than in the analogous Cu(II) system, except for the analyte-free $Co[Au(CN)_2]_2$, which undergoes large structural and visible colour changes upon analyte-binding, albeit slowly. The Ni(II)-based system is relatively inert and does not undergo analyte exchange easily, at least with the analytes tested in this study, although the identity of the analyte present is more easily discerned than for the analogous Co(II) system. Nevertheless, it is clear that a flexible non-porous $M[Au(CN)_2]_2$-superstructure can readily adapt to integrate selected analytes, the efficacy and spectroscopic signatures of which depend on the metal cation in question. An examination of new $M[Au(CN)_2]$-based systems with respect to detecting potential VOC analytes with different donor characteristics is worthwhile and efforts are underway towards this end.

Supplementary Information

Unit cell parameters and powder X-ray diffractogram for $Co[Au(CN)_2]_2$, atomic coordinates for the powder X-ray diffraction models for $Ni[Au(CN)_2]_2(DMF)_2$, $Co[Au(CN)_2]_2(pyridine)_2$, and $Co[Au(CN)_2]_2$, and X-ray crystallographic data in cif format (CCDC Deposition #745836) for $Zn[Au(CN)_2]_2(DMSO)_2$.

Acknowledgments

We are grateful to NSERC of Canada, the World Gold Council GROW program and Simon Fraser University for financial support of this project. JL, JLK and MJK are grateful to NSERC for CGS-D, CGS-M and PGS-D Fellowships respectively.

References

1. White-Morris, R.L.; Olmstead, M.M.; Jiang, F.; Tinti, D.S.; Balch, A.L. Remarkable variations in the luminescence of frozen solutions of $[Au\{C(NHMe)_2\}_2](PF_6)$•0.5(acetone). Structural and spectroscopic studies of the effects of anions and solvents on gold(I) carbene complexes. *J. Am. Chem. Soc.* **2002**, *124*, 2327–2336.
2. Strasser, C.E.; Catalano, V.J. "On Off" Au(I)•••Cu(I) interactions in a $Au(NHC)_2$ luminescent vapochromic sensor. *J. Am. Chem. Soc.* **2010**, *132*, 10009–10011.
3. Lim, S.H.; Olmstead, M.M.; Balch, A.L. Molecular accordion: Vapoluminescence and molecular flexibility in the orange and green luminescent crystals of the dimer, Au_2(μ-bis-(diphenylphosphino)ethane)$_2Br_2$. *J. Am. Chem. Soc.* **2011**, *133*, 10229–10238.

4. Laguna, A.; Lasanta, T.; Lopez-de-Luzuriaga, J.M.; Monge, M.; Naumov, P.; Olmos, M.E. Combining aurophilic interactions and halogen bonding to control the luminescence from bimetallic gold-silver clusters. *J. Am. Chem. Soc.* **2010**, *132*, 456–457.
5. Mansour, M.A.; Connick, W.B.; Lachicotte, R.J.; Gysling, H.J.; Eisenberg, R. Linear chain Au(I) dimer compounds as environmental sensors: A luminescent switch for the detection of volatile organic compounds. *J. Am. Chem. Soc.* **1998**, *120*, 1329–1330.
6. Osawa, M.; Kawata, I.; Igawa, S.; Hoshino, M.; Fukunaga, T.; Hashizume, D. Vapochromic and mechanochromic tetrahedral Gold(I) complexes based on the 1,2-bis(diphenylphosphino)benzene ligand. *Chem. Eur. J.* **2010**, *16*, 12114–12126.
7. Rawashdeh-Omary, M.A.; Omary, M.A.; Fackler, J.P., Jr.; Galassi, R.; Pietroni, B.R.; Burini, A. Chemistry and optoelectronic properties of stacked supramolecular entities of trinuclear gold(I) complexes sandwiching small organic acids. *J. Am. Chem. Soc.* **2001**, *123*, 9689–9691.
8. Fernández, E.J.; Lopez-de-Luzuriaga, J.M.; Monge, M.; Olmos, M.E.; Pérez, J.; Laguna, A.; Mohamed, A.A.; Fackler, J.P., Jr. $\{Tl[Au(C_6Cl_5)_2]\}_n$: A vapochromic complex. *J. Am. Chem. Soc.* **2003**, *125*, 2022–2023.
9. Exstrom, C.L.; Sowa, J.R., Jr.; Daws, C.A.; Janzen, D.; Mann, K.R.; Moore, G.A.; Stewart, F.F. Inclusion of organic vapors by crystalline, solvatochromic $[Pt(arylisonitrile)_4][Pd(CN)_4]$ compounds—Vapochromic environmental sensors. *Chem. Mater.* **1995**, *7*, 15–17.
10. Cich, M.J.; Hill, I.M.; Lackner, A.D.; Martinez, R.J.; Ruthenburg, T.C.; Takeshita, Y.; Young, A.J.; Drew, S.M.; Buss, C.E.; Mann, K.R. Enantiomerically selective vapochromic sensing. *Sens. Actuators B* **2010**, *149*, 199–204.
11. Drew, S.M.; Janzen, D.E.; Buss, C.E.; MacEwan, D.I.; Dublin, K.M.; Mann, K.R. An electronic nose transducer array of vapoluminescent platinum(II) double salts. *J. Am. Chem. Soc.* **2001**, *123*, 8414–8415.
12. Beauvais, L.G.; Shores, M.P.; Long, J.R. Cyano-bridged Re_6Q_8 (Q = S, Se) Cluster-Cobalt(II) framework materials: Versatile solid chemical sensors. *J. Am. Chem. Soc.* **2000**, *122*, 2763–2772.
13. Grove, L.J.; Rennekamp, J.M.; Jude, H.; Connick, W.B. A new class of platinum(II) vapochromic salts. *J. Am Chem. Soc.* **2004**, *126*, 1594–1595.
14. Ley, A.N.; Dunaway, L.E.; Brewster, T.P.; Dembo, M.D.; Harris, T.D.; Baril-Robert, F.; Li, X.; Patterson, H.H.; Pike, R.D. Reversible luminescent reaction of amines with copper(I) cyanide. *Chem. Commun.* **2010**, *46*, 4565–4567.
15. Nassimbeni, L.R.; Kilkenny, M.L. Tetrakis(4-aminopyridine)diisothiocyanatonickel(II) and its clathrates with EtOH, Me_2CO and DMSO: Structures, thermal stabilities and guest exchange. *J. Chem. Soc. Dalton Trans.* **2001**, 1172–1175.
16. Noveron, J.C.; Arif, A.M.; Stang, P.J. Optical sensing of small hydroxyl-containing molecules in new crystalline lamellar arrays of Co(II) and N-(4-pyridyl)benzamide. *Chem. Mater.* **2003**, *15*, 372–374.
17. Gründler, P. *Chemical Sensors: An Introduction for Scientists and Engineers*; Springer: Berlin, Germany, 2007.
18. Buss, C.E.; Anderson, C.E.; Pomije, M.K.; Lutz, C.M.; Britton, D.; Mann, K.R. Structural investigations of vapochromic behavior. X-ray single-crystal and powder diffraction studies of $[Pt(CN\text{-}iso\text{-}C_3H_7)_4][M(CN)_4]$ for M = Pt or Pd. *J. Am. Chem. Soc.* **1998**, *120*, 7783–7790.

19. White-Morris, R.L.; Olmstead, M.M.; Attar, S.; Balch, A.L. Intermolecular interactions in polymorphs of trinuclear gold(I) complexes: Insight into the solvoluminescence of $Au_3(MeN{=}COMe)_3$. *Inorg. Chem.* **2005**, *44*, 5021–5029.
20. Vickery, J.C.; Olmstead, M.M.; Fung, E.Y.; Balch, A.L. Solvent-stimulated luminescence from the supramolecular aggregation of a trinuclear gold(I) complex that displays extensive intermolecular Au-Au interactions. *Angew. Chem. Intl. Ed. Engl.* **1997**, *36*, 1179–1181.
21. Lefebvre, J.; Leznoff, D.B. Structural Diversity, Physical Properties and Applications of Cyanometallate Coordination Polymers. In *Metal and Metalloid-Containing Polymers*; Abd-El-Aziz, A.S., Carraher, C.E., Jr., Pittman, C.U., Jr., Zeldin, M., Eds.; Wiley: New York, NY, USA, 2005; volume 5, pp. 155–208.
22. Cernák, J.; Orendác, M.; Potocnák, I.; Chomic, J.; Orendácová, A.; Skorsepa, J.; Feher, A. Cyanocomplexes with one-dimensional structures: Preparations, crystal structures and magnetic properties. *Coord. Chem. Rev.* **2002**, *224*, 51–66.
23. Shatruk, M.; Avendano, C.; Dunbar, K.R. Cyanide-bridged complexes of transition metals: A molecular magnetism perspective. *Prog. Inorg. Chem*. **2009**, *56*, 155–334.
24. Munoz, M.C.; Real, J.A. Thermo-, piezo-, photo- and chemo-switchable spin crossover iron(II)-metallocyanate based coordination polymers. *Coord. Chem. Rev.* **2011**, *255*, 2068–2093.
25. Sieklucka, B.; Podgajny, R.; Korzeniak, T.; Nowicka, B.; Pinkowicz, D.; Koziel, M. A decade of octacyanides in polynuclear molecular materials. *Eur. J. Inorg. Chem.* **2001**, *2011*, 305–326.
26. Leznoff, D.B.; Xue, B.-Y.; Patrick, B.O.; Sanchez, V.; Thompson, R.C. An aurophilicity-determined 3-D bimetallic coordination polymer: Using $[Au(CN)_2]^-$ to increase structural dimensionality through gold center dot center dot center dot gold bonds in $(tmeda)Cu[Au(CN)_2]_2$. *J. Chem. Soc. Chem. Commun.* **2001**, 259–260.
27. Leznoff, D.B.; Xue, B.-Y.; Batchelor, R.J.; Einstein, F.W.B.; Patrick, B.O. Gold-gold interactions, as crystal engineering design elements in heterobimetallic coordination polymers. *Inorg. Chem.* **2001**, *40*, 6026–6034.
28. Leznoff, D.B.; Lefebvre, J. Coordination polymers with cyanoaurate building blocks: Potential new industrial applications for gold. *Gold Bull.* **2005**, *38*, 47–54.
29. Katz, M.J.; Sakai, K.; Leznoff, D.B. The use of aurophilic and other metal-metal interactions as crystal engineering design elements to increase structural dimensionality. *Chem. Soc. Rev.* **2008**, *37*, 1884–1895.
30. Yam, V.W.-W.; Cheng, E.C.-C. Photochemistry and photophysics of coordination compounds: Gold. *Top. Curr. Chem.* **2007**, *281*, 269–309.
31. Balch, A.L. Remarkable luminescence behaviors and structural variations of two-coordinate gold(I) complexes. *Struct. Bonding (Berlin)* **2007**, *123*, 1–40.
32. Schmidbaur, H.; Schier, A. Aurophilic interactions as a subject of current research: An up-date. *Chem. Soc. Rev.* **2012**, *41*, 370–412.
33. Rawashdeh-Omary, M.A.; Omary, M.A.; Patterson, H.H. Oligomerization of $Au(CN)_2^-$ and $Ag(CN)_2^-$ ions in solution via ground-state aurophilic and argentophilic bonding. *J. Am. Chem. Soc.* **2000**, *122*, 10371–10380.

34. Baril-Robert, F.; Li, X.; Geisheimer, A.; Katz., M.J.; Leznoff, D.B.; Patterson, H.H. Changes in electronic properties of polymeric one-dimensional $\{[M(CN)_2]^-\}_n$ (M = Au, Ag) chains due to neighboring closed-shell Zn(II) or open-shell Cu(II) ions. *Inorg. Chem.* **2011**, *50*, 231–237.
35. Lefebvre, J.; Batchelor, R.J.; Leznoff, D.B. $Cu[Au(CN)_2]_2(DMSO)_2$: Golden polymorphs that exhibit vapochromic behavior. *J. Am. Chem. Soc.* **2004**, *126*, 16117–16125.
36. Leznoff, D.B.; Katz, M.J.; Lefebvre, J. Ammonia-Sensing Cyanoaurate Coordination Polymers. In *Experiments in Green and Sustainable Chemistry*; Roesky, H., Kennepohl, D., Eds.; Wiley: Hoboken, NJ, USA, 2009; Chapter 15, pp. 85–91.
37. Katz, M.J.; Ramnial, T.; Yu, H.Z.; Leznoff, D.B. Polymorphism of $Zn[Au(CN)_2]_2$ and its luminescent sensory response to NH_3 vapor. *J. Am. Chem. Soc.* **2008**, *130*, 10662–10673.
38. Hoskins, B.F.; Robson, R.; Scarlett, N.V.Y. Six interpenetrating quartz-like nets in the structure of $ZnAu_2(CN)_4$. *Angew. Chem. Int. Ed. Engl.* **1995**, *34*, 1203–1204.
39. Rogers, C.W.; Wolf, M.O. Luminescent molecular sensors based on analyte coordination to transition-metal complexes. *Coord. Chem. Rev.* **2002**, *233–234*, 341–350.
40. Lefebvre, J.; Callaghan, F.; Katz, M.J.; Sonier, J.E.; Leznoff, D.B. A new basic motif in cyanometallate coordination polymers: Structure and magnetic behavior of $M(\mu\text{-}OH_2)_2[Au(CN)_2]_2$ (M = Cu, Ni). *Chem. Eur. J.* **2006**, *12*, 6748–6761.
41. Lefebvre, J.; Tyagi, P.; Trudel, S.; Pacradouni, V.; Kaiser, C.; Sonier, J.E.; Leznoff, D.B. Magnetic frustration and spin disorder in isostructural $M(\mu\text{-}OH_2)_2[Au(CN)_2]_2$ (M = Mn, Fe, Co) coordination polymers containing double aqua-bridged chains: SQUID and μSR studies. *Inorg. Chem.* **2009**, *48*, 55–67.
42. Jobbágy, C.; Tunyogi, T.; Pálinkás, G.; Deák, A. A versatile solvent-free mechanochemical route to the synthesis of heterometallic dicyanoaurate-based coordination polymers. *Inorg. Chem*. **2011**, *50*, 7301–7308.
43. Deák, A.; Tunyogi, T.; Pálinkás, G. Synthesis and structure of a cyanoaurate-based organotin polymer exhibiting unusual ion-exchange properties. *J. Am. Chem. Soc.* **2009**, *131*, 2815–2816.
44. Gabe, E.J.; White, P.S.; Enright, G.D. *DIFRAC: A Fortran 77 Control Routine for 4-Circle Diffractometers*; N.R.C.: Ottawa, Canada, 1995.
45. Gabe, E.J.; Page, Y, L.; Charland, J.P.; Lee, F.L.; White, P.S. NRCVAX—An interactive program system for structure-analysis. *J. Appl. Crystallogr.* **1989**, *22*, 384–387.
46. Betteridge, P.W.; Carruthers, J.R.; Cooper, R.I.; Prout, K.; Watkin, D.J. CRYSTALS version 12: Software for guided crystal structure analysis. *J. Appl. Crystallogr.* **2003**, *36*, doi:10.1107/S0021889803021800.
47. Farrugia, L.J. ORTEP-3 for Windows—A version of ORTEP-III with a Graphical User Interface (GUI). *J. Appl. Crystallogr.* **1997**, *30*, doi:10.1107/S0021889897003117.
48. Fenn, T.D.; Ringe, D.; Petsko, G.A. POVScript+: A program for model and data visualization using persistence of vision ray-tracing. *J. Appl. Crystallogr.* **2003**, *36*, 944–947.
49. David, W.I.F.; Shankland, K.; van de Streek, J.; Pidcock, E.; Motherwell, W.D.S.; Cole, J.C. DASH: A program for crystal structure determination from powder diffraction data. *J. Appl. Crystallogr.* **2006**, *39*, 910–915.

50. Colacio, E.; Lloret, F.; Kivekäs, R.; Ruiz, R.; Suárez-Varela, J.; Sundberg, M.R. Aurophilicity as a cofactor in crystal engineering. Dicyanoaurate(I) anion as a building block in a novel Co(II)-Au(I) bimetallic assembly. *Chem. Commun.* **2002**, 592–593.
51. Roisnel, T.; Rodriguez-Carvajal, J. WinPLOTR: A Windows Tool for Powder Diffraction Pattern Analysis. In *Proceedings of the Seventh European Powder Diffraction Conference (EPDIC 7)*, Barcelona, Spain, 20–23 May 2000; pp. 118–123.
52. Nakamoto, K. *Infrared and Raman Spectra of Inorganic and Coordination Compounds*, 5th ed.; John Wiley & Sons: New York, NY, USA, 1997.
53. Dunbar, K.R.; Heintz, R.A. Chemistry of transition metal cyanide compounds: Modern perspectives. *Prog. Inorg. Chem.* **1997**, *45*, 283–391.
54. Dong, W.; Zhu, L.-N.; Sun, Y.-Q.; Liang, M.; Liu, Z.-Q.; Liao, D.-Z.; Jiang, Z.-H.; Yan, S.-P.; Cheng, P. 3D porous and 3D interpenetrating triple framework structures constructed by aurophilicity-coordination interplay in $\{Mn[Au(CN)_2]_2(H_2O)_2\}_n$ and $\{KFe[Au(CN)_2]_3\}_n$. *Chem. Commun.* **2003**, 2544–2545.
55. Abrahams, S.C.; Zyontz, L.E.; Bernstein, J.L. Cobalt Cyanoaurate—Crystal structure of a component from cobalt-hardened gold electroplating baths. *J. Chem. Phys.* **1982**, *76*, 5458–5462.
56. Katz, M.J.; Aguiar, P.M.; Batchelor, R.J.; Bokov, A.; Ye, Z.-G.; Kroeker, S.; Leznoff, D.B. Structure and multinuclear solid-state NMR of a highly birefringent lead-gold cyanide coordination polymer. *J. Am. Chem. Soc.* **2006**, *128*, 3669–3676.
57. Lefebvre, J.; Chartrand, D.; Leznoff, D.B. Synthesis, structure and magnetic properties of 2-D and 3-D [cation]$\{M[Au(CN)_2]_3\}$ (M = Ni, Co) coordination polymers. *Polyhedron* **2007**, *26*, 2189–2199.
58. Atwood, J.L.; Barbour, L.J.; Jerga, A.; Schottel, B.L. Guest transport in a nonporous organic solid via dynamic van der Waals cooperativity. *Science* **2002**, *298*, 1000–1002.
59. Batten, S.R.; Murray, K.S. Malleable coordination networks. *Aust. J. Chem.* **2001**, *54*, 605–609.
60. Côté, A.P.; Shimizu, G.K.H. The first example of a functional pillared metal sulfonate network. *Chem. Commun*. **2001**, 251–252.
61. Côté, A.P.; Ferguson, M.J.; Khan, K.A.; Enright, G.D.; Kulynych, A.D.; Dalrymple, S.A.; Shimizu, G.K.H. Intercalation of alcohols in Ag sulfonates: Topotactic behavior despite flexible layers. *Inorg. Chem*. **2002**, *41*, 287–292.
62. Kitagawa, S.; Kitaura, R.; Noro, S.-I. Functional porous coordination polymers. *Angew. Chem. Int. Ed.* **2004**, *43*, 2334–2375.
63. Horike, S.; Shimomura, S.; Kitagawa, S. Soft porous crystals. *Nat. Chem*. **2009**, *1*, 695–704.
64. Kajiro, H.; Kondo, A.; Kaneko, K.; Kanoh, H. Flexible two-dimensional square-grid coordination polymers: Structures and functions. *Int. J. Mol. Sci.* **2010**, *11*, 3803–3845.